Formamidinium-Based Dion-Jacobson Layered Hybrid Perovskites: Structural Complexity and Optoelectronic Properties

María C. Gélvez-Rueda, Paramvir Ahlawat, Lena Merten, Farzaneh Jahanbakhshi, Marko Mladenović, Alexander Hinderhofer, M. Ibrahim Dar, Yang Li, Algirdas Dučinskas, Brian Carlsen, Wolfgang Tress, Amita Ummadisingu, Shaik M. Zakeeruddin, Frank Schreiber, Anders Hagfeldt, Ursula Rothlisberger,* Ferdinand C. Grozema,* Jovana V. Milić,* and Michael Graetzel*

Layered hybrid perovskites have emerged as a promising alternative to stabilizing hybrid organic–inorganic perovskite materials, which are predominantly based on Ruddlesden-Popper structures. Formamidinium (FA)-based Dion-Jacobson perovskite analogs are developed that feature bifunctional organic spacers separating the hybrid perovskite slabs by introducing 1,4-phenylenedimethanammonium (PDMA) organic moieties. While these materials demonstrate competitive performances as compared to other FA-based low-dimensional perovskite solar cells, the underlying mechanisms for this behavior remain elusive. Here, the structural complexity and optoelectronic properties of materials featuring $(PDMA)FA_{n-1}Pb_nI_{3n+1}$ ($n = 1-3$) formulations are unraveled using a combination of techniques, including X-ray scattering measurements in conjunction with molecular dynamics simulations and density functional theory calculations. While theoretical calculations suggest that layered Dion-Jacobson perovskite structures are more prominent with the increasing number of inorganic layers (n), this is accompanied with an increase in formation energies that render $n > 2$ compositions difficult to obtain, in accordance with the experimental evidence. Moreover, the underlying intermolecular interactions and their templating effects on the Dion-Jacobson structure are elucidated, defining the optoelectronic properties. Consequently, despite the challenge to obtain phase-pure $n > 1$ compositions, time-resolved microwave conductivity measurements reveal high photoconductivities and long charge carrier lifetimes. This comprehensive analysis thereby reveals critical features for advancing layered hybrid perovskite optoelectronics.

1. Introduction

Hybrid organic–inorganic halide perovskites have taken the leading role in the research on thin film photovoltaics over the past decade.[1–3] Their structural versatility enables a wide range of applications in various optoelectronic devices, such as light emitting diodes, photodetectors, photocatalysts, and others.[1–3] However, these materials have shown limited stability against oxygen and water,[4–6] which has increased the interest in low-dimensional perovskite analogues.[7–11] Layered 2D perovskites incorporate hydrophobic organic cations between the hybrid perovskite slabs that are mainly defined by $S_2A_{n-1}Pb_nX_{3n+1}$ and $S'A_{n-1}Pb_nX_{3n+1}$ formulations, where S and S' are mono- and bifunctional organic spacers, respectively, A is the organic cation in the perovskite slab (such as methylammonium (MA) or formamidinium (FA)), M is a divalent metal (mostly Pb^{2+}), and X is the halide anion (Cl^-, Br^-, or I^-), while n defines the number of hybrid perovskite slabs.[9–13] It is worth noting that, although we refer to these formulations as low-dimensional perovskites in accordance with the conventional nomenclature,[8,9] some

Dr. M. C. Gélvez-Rueda, Prof. F. C. Grozema
Department of Chemical Engineering
Delft University of Technology
Delft 2629 HZ, The Netherlands
E-mail: f.c.grozema@tudelft.nl

The ORCID identification number(s) for the author(s) of this article can be found under https://doi.org/10.1002/adfm.202003428.

[+]Present address: Department of Physics, Cavendish Laboratory, JJ Thomson Avenue, Cambridge CB3 0HE, UK

P. Ahlawat, F. Jahanbakhshi, Dr. M. Mladenović, Prof. U. Rothlisberger
Laboratory of Computational Chemistry and Biochemistry
Institute of Chemical Sciences and Engineering
Ecole Polytechnique Fédérale de Lausanne
Lausanne 1015, Switzerland
E-mail: ursula.roethlisberger@epfl.ch

L. Merten, Dr. A. Hinderhofer, Prof. F. Schreiber
Institut für Angewandte Physik
Universität Tuebingen
Auf der Morgenstelle 10, Tübingen 72076, Germany

**ADVANCED
SCIENCE NEWS**
www.advancedsciencenews.com

**ADVANCED
FUNCTIONAL
MATERIALS**
www.afm-journal.de

of these materials might not strictly correspond to perovskite structures and they could be more appropriately denoted as perovskite-related structures.[10] In addition to their classification by the number of slabs ($n = 1, 2, 3$, etc.), two main archetypes of layered perovskites are predominant to date, namely Ruddlesden-Popper (RP) and Dion-Jacobson (DJ) systems.[9–20] The RP structural category is defined by the $S_2A_{n-1}Pb_nX_{3n+1}$ formulation, which comprises an organic double layer between the inorganic layers featuring an offset per unit cell of the perovskite slab.[9–12] The DJ systems are based on the $S'A_{n-1}Pb_nX_{3n+1}$ compositions employing organic layers (S') that stack in an almost perfect alignment between unit cells, featuring smaller interlayer space.[15–20] Reducing interlayer distances and tuning their mutual alignment are important parameters for controlling the optoelectronic properties as they strengthen electronic interactions between the inorganic layers and, consequently, facilitate interlayer charge transport, rendering the DJ structures superior to RP phases.[15–20] Most of the developments of layered hybrid perovskites are based on RP archetypes and there are very few examples of hybrid DJ architectures to date.[15–20] This is particularly the case for FA-containing layered perovskites, which are relatively unexplored despite the superior thermal stabilities of FA-based hybrid perovskite compositions.[4,14,16,21–25]

We have recently shown the possibility to form Dion-Jacobson hybrid perovskites with 1,4-phenylenedimethanammonium (PDMA) spacer moieties (**Figure 1**).[16] This system has been proven effective in forming low compositional ($n = 1$) layered structures, whereas featuring mixed phases for $n > 1$ representatives.[16] Such phase mixtures are commonly observed for 2D hybrid perovskites, where obtaining phase purity is an ongoing challenge.[16,24,26–29] Nonetheless, materials based on $(PDMA)FA_{n-1}Pb_nX_{3n+1}$ compositions ($n = 1–3$) have demonstrated promising photovoltaic performances in conventional mesoscopic (mp) n–i–p device architectures as compared to other $FAPbI_3$-based low-dimensional perovskite solar cells with light-to-electric power conversion efficiencies exceeding 7%.[8,16,22] This was accompanied by long-term stabilities, which were achieved with thin (≈200 nm) films of active materials under room temperature deposition, thus surpassing the performances of $FAPbI_3$-based perovskite solar cells with 2D compositions reported to date.[16,22,24]

In this work, we unravel the underlying structural complexity and optoelectronic properties of Dion-Jacobson perovskites based on $(PDMA)FA_{n-1}Pb_nI_{3n+1}$ ($n = 1–3$) compositions. This system was investigated by X-ray scattering measurements in conjunction with molecular dynamics simulations and density functional theory calculations, as well as UV–vis absorption and photoluminescence spectroscopy and microwave conductivity

measurements. We experimentally demonstrate the formation of layered perovskite structures, although obtaining phase-pure $n > 1$ compositions remains challenging. The latter is rationalized by our computational studies that show that increasingly endothermic formation enthalpies with increasing number of inorganic layers (n) obstruct the realization of $n > 2$ compositions. Combining the experimental and computational results, we elucidate the intermolecular interactions associated with Dion-Jacobson structures and show that subtle templating effects involving both the organic and the inorganic component are responsible for the structural properties. This results in reduced distances and improved alignment between neighboring layers, which directly affects the electronic properties. Accordingly, despite challenges to obtain phase-pure $n > 1$ compositions, time-resolved microwave conductivity measurements reveal high photoconductivities and long charge carrier lifetimes that highlight the promising use of these materials in optoelectronics.

2. Results and Discussion

We have analyzed thin films of $(PDMA)FA_{n-1}Pb_nI_{3n+1}$ ($n = 1–3$) compositions that are prepared by solution deposition using
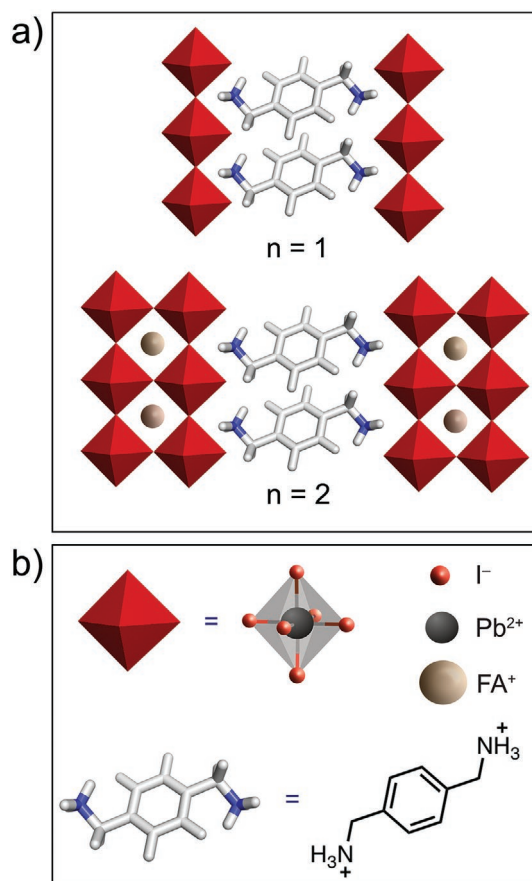
Dr. M. I. Dar, Dr. Y. Li, A. Dučinskas, Dr. A. Ummadisingu,[+]
Dr. S. M. Zakeeruddin, Dr. J. V. Milić, Prof. M. Graetzel
Laboratory of Photonics and Interfaces
Institute of Chemical Sciences and Engineering
Ecole Polytechnique Fédérale de Lausanne
Lausanne 1015, Switzerland
E-mail: jovana.milic@epfl.ch; michael.graetzel@epfl.ch
B. Carlsen, Dr. W. Tress, Prof. A. Hagfeldt
Laboratory of Photomolecular Science
Institute of Chemical Sciences and Engineering
Ecole Polytechnique Fédérale de Lausanne
Lausanne 1015, Switzerland

Figure 1. Schematic representation of Dion-Jacobson layered hybrid perovskites. a) Envisaged structure of layered perovskites based on $(PDMA)FA_{n-1}Pb_nI_{3n+1}$ composition incorporating 1,4-phenylenedimethanammonium cations with b) structural details.

stoichiometric amounts of the precursors (PDMAI$_2$, FAI, and PbI$_2$) in ratios defined by the reported compositions (n). The resulting formulations are based on the stoichiometry of the precursors without assumptions regarding the resulting crystal structure. The precursors are dissolved in a mixture of *N,N*-dimethylformamide (DMF) and dimethyl sulfoxide (DMSO) in a 9:1 volume ratio in accordance with the previously optimized procedure.[16] The precursor solution was spin-coated at ambient temperature on the corresponding substrate, which was followed by subsequent annealing at 150 °C, as detailed in the Supporting Information. The analysis focused on two substrates, namely fluorine doped tin oxide (FTO) coated with either mp-TiO$_2$, which has been previously employed in photovoltaic devices, or mp-Al$_2$O$_3$, which is used as a nonelectroactive mesoscopic analogue for the analysis of the optoelectronic properties.[16,24] Moreover, quartz substrates are used to reliably assess photoconductivities of the materials.[30,31]

Structural properties of thin films were investigated by means of X-ray reflectivity (XRR) and grazing incidence X-ray scattering (GIXS) techniques. XRR patterns of the thin films of (PDMA)FA$_{n-1}$Pb$_n$I$_{3n+1}$ (n = 1–3) compositions on FTO/mp-TiO$_2$ substrates suggest formation of low-dimensional hybrid perovskite structures, which are revealed by the presence of distinct signals in the q_z-range below 1 Å^{-1} ($2\theta < 10°$), that are commonly ascribed to the (001) planes (**Figure 2**a and Figure S1, Supporting Information).[12,13,15,16] Films based on n = 1 compositions revealed strong signals at q_z = 0.5 Å^{-1} and q_z = 1 Å^{-1}, indicative for an out-of-plane layered structure. The n = 1 structure is characterized by the d-spacing of 12.5 Å, that corresponds to the q-value of the first maximum, which is in line with the layered phase stacked parallel to the substrate (inset of Figure 2c). This feature is, however, only weakly observed for n > 1 compositions (Figure 2 and Figures S1 and S2, Supporting Information). Radial integration of grazing incidence wide-angle X-ray scattering (GIWAXS) patterns (**Figure 3**d) as well as grazing incidence X-ray diffraction (GIXD) measurements (see Figures S1 and S2 in the Supporting Information) reveal that n = 2 compositions feature additional signals at q_z = 0.33 Å^{-1} and q_z = 0.67 Å^{-1}, indicative of the formation of distinct n = 2 layered structures, whereas n > 2 compositions were closely comparable to each other irrespective of the stoichiometry of the precursors (Figure 3d and Figures S1 and S2, Supporting Information). Moreover, for n = 2 composition, the n = 1 structure appears to be present in addition to the newly formed 2D phase, while the sample also features a cubic α-FAPbI$_3$ perovskite phase. This is in accordance with the previously reported formation of phase mixtures for n > 1 compositions in layered hybrid perovskites.[16,24,26–29] The intensity of the cubic α-FAPbI$_3$ perovskite phase in the diffraction pattern increases for n > 2 compositions, along with the presence of hexagonal δ-FAPbI$_3$ phase. Furthermore, the diffraction patterns for n = 3 compositions reveal presence of both n = 1 and n = 2 phases, along with the 3D α-FAPbI$_3$ perovskite phase, possible traces of PbI$_2$, as well as δ-FAPbI$_3$ phase, which additionally supports the complexity of the phase mixtures (Figure 3d and Figures S1 and S2, Supporting Information).[16,24] However, apart from signals associated with the 3D α-FAPbI$_3$ and δ-FAPbI$_3$ phases, the nominal n = 3 composition did not reveal presence of any addi-

tional phases that can be directly ascribed to the formation of n > 2 representatives (Figures 2 and 3; Figures S1 and S2, Supporting Information).

To understand this absence of the apparent n > 2 phases under applied experimental conditions, as well as to further evaluate structural properties of these systems, we conducted a theoretical investigation of their structural and optoelectronic properties. For this purpose, classical molecular dynamics (MD) simulations were performed, followed by density functional theory (DFT) calculations for various perovskite compositions (n = 1–3; for computational details refer to the Sections S2 and S3 of the Suporting Information). During the MD simulations for n = 1 compositions, a transition from what appears to be a mixed DJ-RP structural intermediate to a pure DJ structure occurs at higher temperatures (>350 K; Figure S5, Supporting Information). Furthermore, the rotation of the spacer is significantly faster for n > 1 as compared to the n = 1 compositions (Figure S6, Supporting Information). The optimization process further suggests that n > 1 compositions do not display any apparent temperature-dependent transition as the system persists in a DJ structure, approaching a near-ideal DJ structure with increasing number of inorganic layers (n). This is the result of the complex interplay between the inorganic and organic parts of the material. Unlike the alkyl-based spacer groups that feature weaker van der Waals interactions,[19] the intermolecular interactions in the aromatic PDMA spacer layer were found to adopt both T-shaped and parallel-displaced stacking π interactions (Figures S7 and S8, Supporting Information), leading to a more rigid inorganic framework, which was assumed to be associated with the templating effect.[32]

To probe possible templating effects of the spacer layer on the inorganic framework, we analyzed the average tilting angle between Pb–I octahedra, as well as the penetration depths of the spacers into the inorganic part by DFT calculations. The latter was assessed by following the distance between the nitrogen atoms of the amino group of the spacer (N) and the nearest inorganic slab Pb positions. We further analyzed the hydrogen bond length between amino group nitrogen atoms of each spacer and the nearest iodide ions of the same inorganic slab (N···I distance), which has previously been used as an indicator of structural stability.[33] Based on the DFT-optimized structures, increasing the number of inorganic layers (increasing n) leads to an increase in the penetration depth, which corresponds to a decrease of the N···Pb distances. This results in the inorganic layer becoming more cubic, which is indicated by the interoctahedral tilting angles approaching 90°.[34] Consequently, the voids between octahedra widen and thus the iodide ions are placed further away from the ammonium groups, leading to an apparent increase of the N···I distances, further suggestive of a templating effect in the inorganic layer.[34] To inspect whether this leads in turn to changes in the organic spacer layer, we analyzed its thickness by monitoring the average Pb···Pb distances between opposite layers (d_1) as well as the π–π distances between the aromatic rings (d_2) (Figure 2b, Figure S8 and Table S2, Supporting Information). Similar to the behavior of alkyl-based BA and 5-ammonium valeric acid (5-AVA) layered RP perovskite systems,[34] the interlayer distance (d_1) was found to decrease upon deeper incorporation of the organic cation into the inorganic layer,
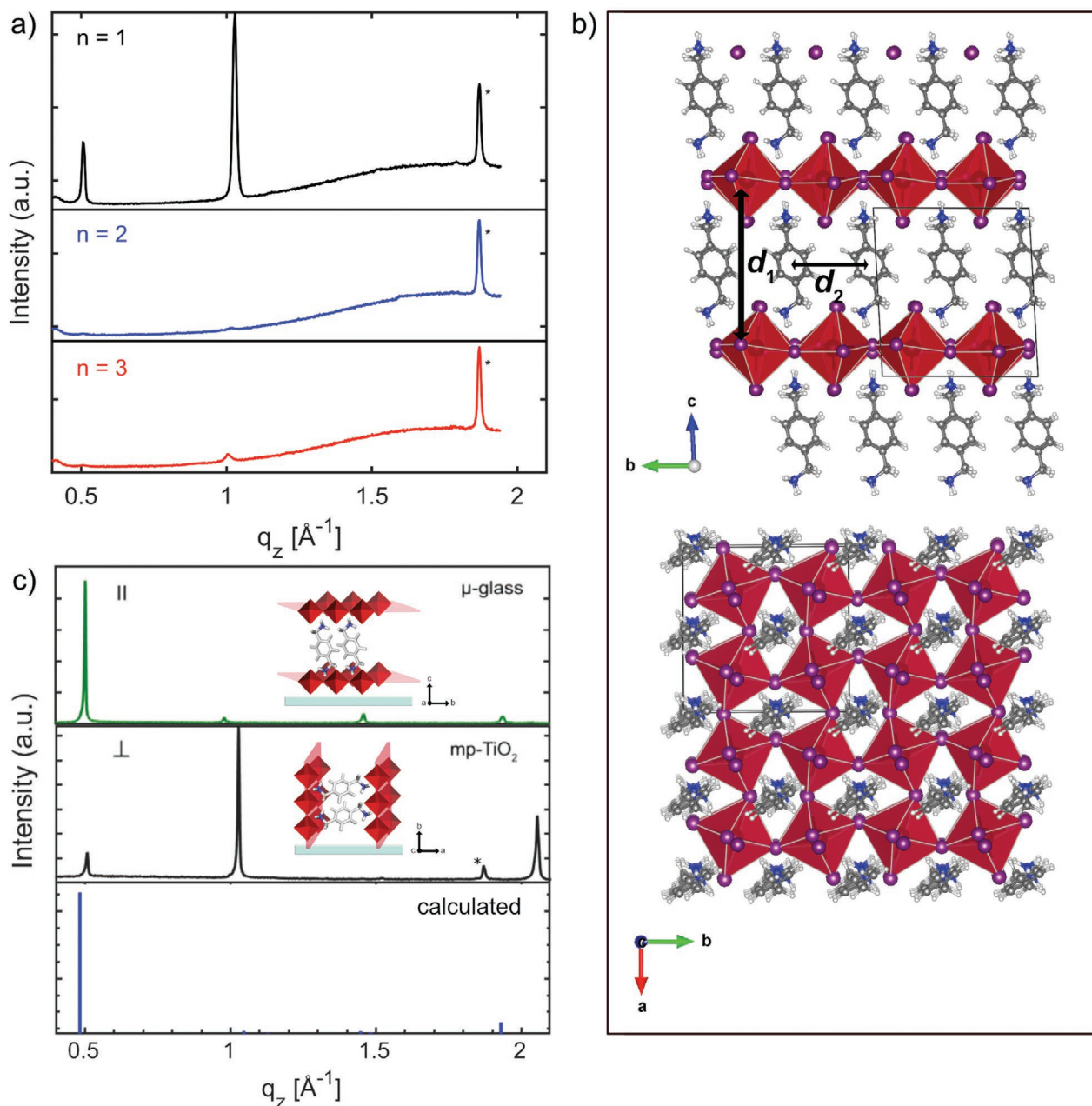
Figure 2. Structural properties of thin films based on $(PDMA)FA_{n-1}Pb_nI_{3n+1}$ composition. a) XRR patterns on FTO/mp-TiO$_2$ substrates for $n = 1$ (black), $n = 2$ (blue) and $n = 3$ (red) compositions. b) DFT-calculated structure of $n = 1$ composition (d_1 and d_2 are the characteristic intra and inter-layer distances). More details are shown in Sections S3 and S4 of the Supporting Information. c) Comparison of DFT-simulated (blue) with the experimental XRD patterns of (PDMA)PbI$_4$ ($n = 1$) layered structure on either microscopic glass (green) or FTO/mp-TiO$_2$ (black) substrates. The inset shows schematic representations of parallel (∥) and perpendicular (⊥) orientations of the system with respect to the substrate, commonly associated with $q_z < 1$ Å^{-1} ($2\theta < 10°$) and around 1 Å^{-1} (2θ around 14°), respectively. Asterisks denote substrate peaks.

which also evidences a templating effect between inorganic slabs and the spacer layer.[32] Moreover, the decrease of the inter-layer distances is further pronounced for the DJ phases as compared to the RP ones,[19] particularly for spacer groups that feature stronger noncovalent interactions, such as the π-based interactions evidenced for the PDMA spacer. The effect that the organic component has on interlayer distances and alignment of the adjacent layers offers a particularly important approach

to optimize the optoelectronic properties, as these structural parameters are directly related to increasing orbital interactions that facilitate inter-layer charge transport.[15–20]

These structural changes are assumed to be apparent in the experimentally obtained thin films. We thereby simulated the XRD patterns for the calculated (PDMA)PbI$_4$ structures and compared them to the experimental ones (Figure 2c). The patterns were closely comparable, featuring lowest angle peaks that
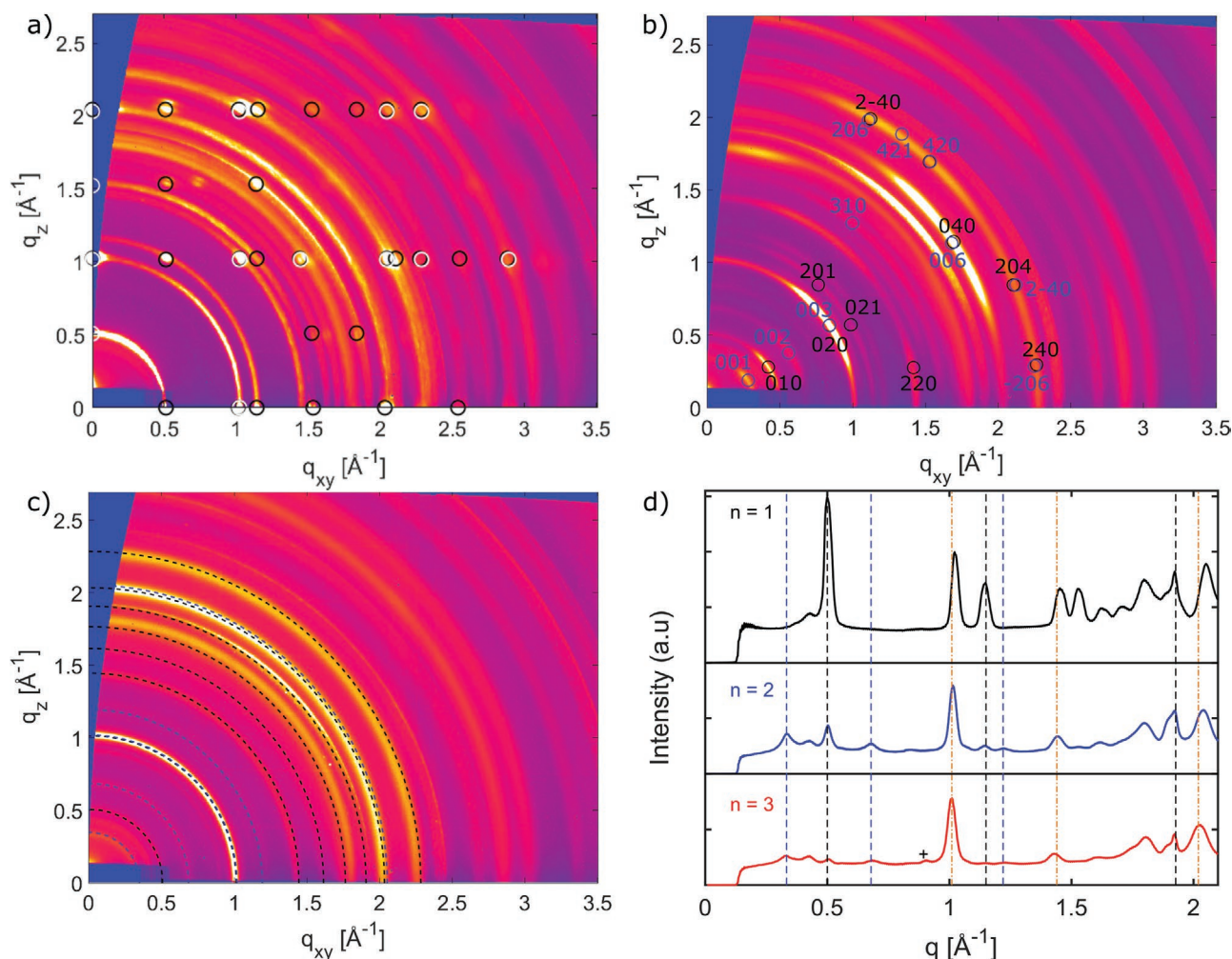
Figure 3. Crystal structure analysis and orientation in thin films. a–c) GIWAXS reciprocal space maps ($\alpha_i = 0.1°$) for perovskite thin films based on (PDMA)FA$_{n-1}$Pb$_n$I$_{3n+1}$ formulation with a) $n = 1$, b) $n = 2$ and c) $n = 3$ compositions on FTO/mp-TiO$_2$ substrates. Spot patterns in a) suggest well-defined orientations, while peaks from $n = 1$ structure oriented perpendicular (parallel) to the substrate are indicated in black (white) circles. Ring-shaped features with angular maxima in b) indicate preferred orientation, while black (blue) circles indicate layered $n = 1$ ($n = 2$) structure. Uniform angular intensity distribution in c) is in accordance with random orientation of crystallites corresponding to $n = 1$ and $n = 2$ structures, which are indicated by black and blue lines, respectively. d) Radially integrated intensities of the q-maps for nominal $n = 1$ (black), $n = 2$ (blue) and $n = 3$ (red) composition. Signals originating from distinct $n = 1$ and $n = 2$ structures are indicated by vertical dashed lines in black and blue, respectively. Yellow vertical dot-dashed lines indicate a cubic perovskite structure, while + marks PbI$_2$ phase. Angular intensity distributions can be found in Figure S3 (Supporting Information).

correspond to real space interlayer distances of 13 and 12.4 Å for calculated and experimental values, respectively. This confirms that the computational models are in good agreement with experimentally obtained systems (Figure 2c).

In the experimental system, however, the anisotropic nature of the layered hybrid perovskite structure enables formation of multiple orientations with respect to the substrate that further affect the properties of these systems. In this regard, two distinct orientations are important, namely the parallel (∥) and the perpendicular (⊥) orientations (Figure 2c, inset). Lower compositional representatives ($n = 1$) are known to feature predominantly ∥ orientations (Figure 2c), whereas higher compositional representatives ($n > 1$) form ⊥ orientations that are more relevant for photovoltaics.[9,12,14] The former orientations are commonly revealed through the appearance of (001) plane reflections at $q_z < 1$ Å^{-1} ($2\theta < 10°$), while the latter ones

lead to the appearance of the reflections of the (111) plane at q_z around 1 Å^{-1} (2θ of ≈14–15°). The predominant phase can be further controlled by the experimental conditions (e.g., using additives, hot-casting technique, and other methods).[9,12] The orientations with respect to the FTO/mp-TiO$_2$ substrates were analyzed by grazing incidence wide angle X-ray scattering (GIWAXS; Figure 3 and Figures S2–S4, Supporting Information), which indicates well-oriented layered structures for $n = 1$ compositions with a certain number of disordered domains (Figure 3a, Figures S3a and S4, Supporting Information). Moreover, the $n = 2$ compositions show ring shaped features with angular maxima, suggesting a preferred orientation (Figure 3b and Figure S3b, Supporting Information. Conversely, $n > 2$ compositions feature uniform angular intensity distribution that can be associated with a random orientation of crystallites (Figure 3c and Figure S3, Supporting
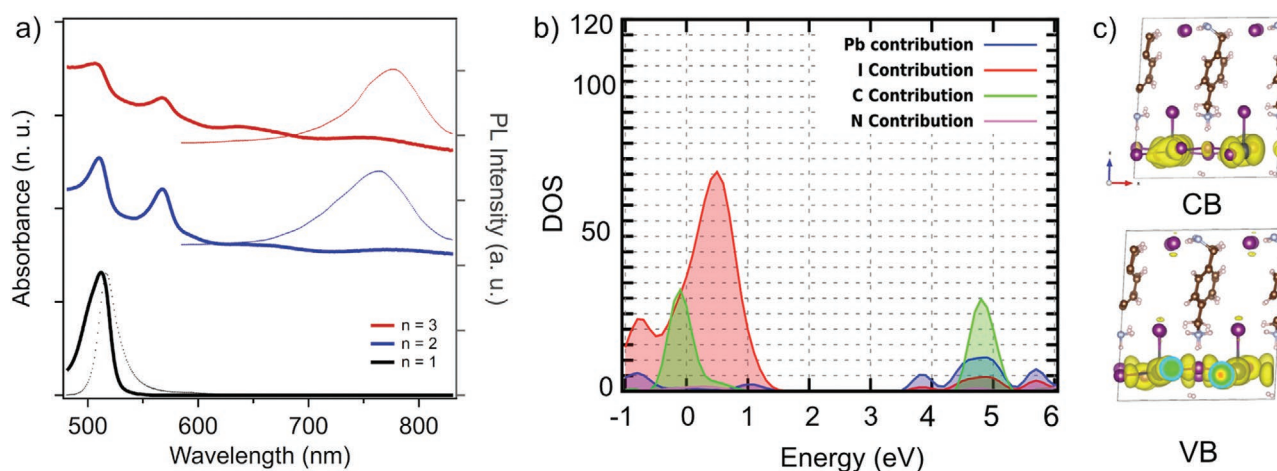
Figure 4. Optoelectronic properties of perovskite thin films. a) UV–vis absorption (solid lines, left) and photoluminescence (PL, dashed, right) spectra of thin films based on (PDMA)FA$_{n-1}$Pb$_n$I$_{3n+1}$ formulation ($n = 1–3$) on FTO/mp-Al$_2$O$_3$ substrates in accordance with the previous report.[16] b) Calculated partial density of states and c) Frontier molecular orbitals (top of the valence band (VB, bottom) and bottom of the conduction band (CB, top)) for (PDMA)PbI$_4$.

Information), featuring $n = 1$ and $n = 2$ compositions. The well-defined orientation of $n = 1$ compositions enables estimating the unit cell parameters, which were found to match well with the theoretical model, while featuring a minor deviation of the unit cell angles from the ideal cubic structure (Figure S4 and Table S1, Supporting Information). This provides further validation for the theoretical model. However, the challenge lies in the formation of higher compositional ($n > 2$) representatives, which have not been unambiguously evidenced under the applied experimental conditions in this work. To scrutinize the lack of formation of $n > 2$ phases, we calculated the formation energies by DFT calculations for theoretical models of $n = 1–3$ systems with respect to the precursors (PbI$_2$, FAI, and PDMAI$_2$). We found the $n = 1$ structure exhibits the lowest (essentially thermoneutral) formation energy (-0.00 eV per f.u.), which is higher for $n > 1$ compositions (0.21 eV per f.u. for $n = 2$ and 0.30 eV per f.u. for $n = 3$), indicating relative instability of higher ($n > 1$) compositional representatives with respect the $n = 1$ system and α-FAPbI$_3$, which exhibits the formation energy of 0.08 eV per f.u. (Figure S8, Supporting Information). This could potentially be circumvented by introducing smaller ions in the composition, such as Cs and Br, which can stabilize the perovskite (α) FAPbI$_3$ phase, and consequently, could facilitate the formation of higher compositional ($n > 2$) representatives.[21,35]

The resulting structural features directly affect the optoelectronic properties of the system, which were analyzed experimentally by UV–vis absorption and steady-state photoluminescence (PL) emission spectroscopy (**Figure 4a**). The spectra reveal a trend in optical bandgap energy (E_g) that has been previously reported and is typical of low-dimensional perovskites, as it decreases with the increase in the relative number of inorganic slabs (n, Figure 4a).[12,14,26,35–37] Moreover, the UV–vis absorption spectra show characteristic excitonic features, which disappear with an increase in the number of inorganic layers (n, Figure 4a) and is likely due to the increasing contribution of the 3D perovskite phase.[13,38] These features can also serve as a qualitative indicator for the presence of a certain structural phase and, in this regard, the $n = 1$ compositions show

well-defined optical signatures (Figure 4a, black), whereas $n > 1$ compositions reveal multiple signals in the UV–vis absorption spectra accompanied by a large Stokes shift in the PL spectra (Figure 4a, red and blue). This is in accordance with the presence of a mixture of phases and the coexistence of 3D FAPbI$_3$ perovskite phase,[16,24] as confirmed by the XRR and GIWAXS measurements. Accordingly, PL spectra of the films based on higher $n > 1$ compositions display emission around 770 nm whereas those based on lower $n = 1$ compositions feature the main emission at around 550 nm (Figure 4a), similarly to the other reported DJ phases.[15,17] DFT-calculated bandgaps (for details see Section S3, Supporting Information) follow the expected trend as a function of n and yield a value for (PDMA)PbI$_4$ of 2.8 eV, which is 0.4 eV larger than the experimental optical gap due to excitonic contributions (Table S3, Supporting Information).[16] Indeed, this energy difference is consistent with the reported exciton binding energies for 2D perovskites, which are in the order of 380 meV.[30,38] Furthermore, the effective masses in the in-plane directions decrease with increasing n (Tables S2 and S3, Supporting Information). As expected, significantly higher values of effective masses are observed in the perpendicular direction to the inorganic layer. However, the results of the calculations of the partial density of states (Figure 4b), as well as the frontier molecular orbitals (Figure 4c), exclude a direct contribution of the organic part to the band edges. Nevertheless, the values for effective masses, especially in the perpendicular direction, are smaller than some of the representative RP phases.[34] This is likely due to reduced interlayer distances and better alignment of inorganic layers in the DJ structure, which results in improved charge transport and optoelectronics.

The charge carrier dynamics were investigated by time-resolved microwave conductivity (TRMC) measurements. In these measurements, high-frequency microwaves are used to probe the change in the conductivity of materials due to generated mobile charge carriers. Mobile charge carriers absorb a fraction of the incoming microwave power (ΔP), which is proportional to the change in the conductivity of the material
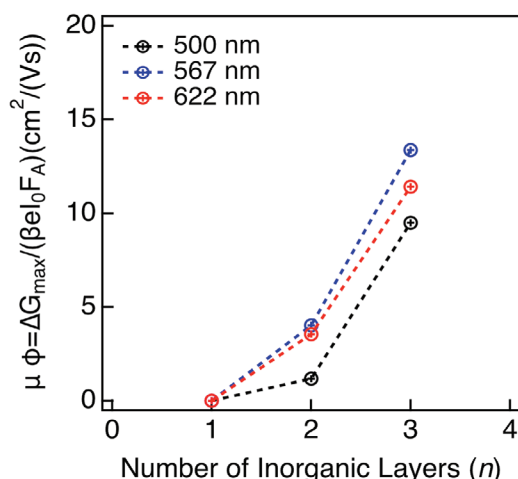
Figure 5. Maximum photoconductivity of thin films at 298 K based on (PDMA)FA$_{n-1}$Pb$_n$I$_{3n+1}$ composition (n = 1–3) excited at the respective excitonic wavelengths (500, 567, and 622 nm) of n = 1 (black), n = 2 (blue) and n = 3 (red), respectively.

($\Delta\sigma$). It is possible to generate charge carriers using either a high energy electron pulse (pulse-radiolysis, PR-TRMC) or by laser excitation (photoconductivity TRMC).[30] PR-TRMC is used to determine the mobility of charge carriers on materials in crystal form. The high-energy electron pulse assures the generation of free charge carriers (i.e., electrons and holes), independently of the exciton binding energy of the material.[30] The mobility of charge carriers was measured on powders of layered hybrid perovskites of different compositions (n = 1–3) synthesized mechanochemically. However, the powder samples prepared by this method exhibit a large concentration of defects that obscure the mobility and charge carrier dynamics on these materials (Figures S10 and S11, Supporting Information).[31]

In a separate experiment, we used the TRMC technique together with photoexcitation with a nanosecond laser pulse to analyze photoinduced conductivity in thin films based (PDMA)FA$_{n-1}$Pb$_n$I$_{3n+1}$ (n = 1–3) compositions of ≈200 nm thickness. The photoconductivity signal that is measured is directly influenced by the exciton binding energy of the material.[30] As a result, the photoconductivity obtained from the TRMC experiment is the product of charge mobility (μ) and quantum yield of free charge carrier formation (φ) in accordance with the Equation (1).

$$\varphi \sum \mu = \frac{\Delta G_{max}}{I_0 \beta e F_A} \qquad (1)$$

Here, ΔG_{max} is the maximum photoconductance, I_0 is the number of photons per unit area per pulse, β is defined by the dimensions of the microwave cavity, e is the elementary charge, whereas F_A is the fraction of photons that is absorbed by the sample.

The samples were photoexcited at three different wavelengths that correspond to the excitonic peaks of the different number of inorganic layers (Figure 4a), namely 500 nm (n = 1), 560 nm for (n = 2) and 622 nm (n = 3). The photoconductivity was found to increase with the number of inorganic layers (n; **Figure 5**b), which is in accordance with the reduction of the

effective masses revealed by DFT calculations, as well as a gradual decrease in the exciton binding energy, which will result in an increase of the yield of dissociation of charge carriers (φ).[30] The photoconductivity for n = 3 compositions is found to be at the order of magnitude of 3D FAPbI$_3$ films measured with the same technique (8–60 cm^2 V^{-1} s^{-1}; Figure 5b and Figure S11, Supporting Information). However, the n = 3 composition contains a mixture of FAPbI$_3$ with n = 2 and n = 1 layers, hence the high photoconductivity is likely affected by the 3D FAPbI$_3$ phase. The photoconductivity for the n = 2 composition is around 4 cm^2 V^{-1} s^{-1}, which is an order of a magnitude higher than 2D Ruddlesden-Popper n = 2 (e.g. BA$_2$Pb$_2$I$_7$) phase[30] and a value suitable for photovoltaic applications. The presence of 3D FAPbI$_3$ is to a large extent responsible for this high, long-lived photoconductivity signal (shown in Figure S11 of the Supporting Information). In the case of the n = 1 material, the photoconductivity is comparable to pure 2D Ruddlesden-Popper layered perovskite systems (0.1–0.3 cm^2 V^{-1} s^{-1}).[30]

We further analyzed the charge carrier dynamics in thin films to find that the height of the photoconductivity and lifetime signal for n = 1–3 compositions decrease as the photon intensity increases, following a second order behavior (Figure S12, Supporting Information). In addition, it is clear that the lifetime increases with the number of inorganic layers, exhibiting a long-lived component for n > 1 compositions in the order of 20 µs for n = 2 and 15 ms for n = 3 compositions (**Figure 6**). This long-lived component is longer than the lifetime observed for 3D FAPbI$_3$ perovskites (Figure S11, Supporting Information). At these longer time scales, the decay traces for n = 2 compositions seem to show a second order behavior (Figure 6a), whereas for n = 3 composition a first order behavior is apparent, the lifetime of carriers being independent of their initial concentration (Figure 6b).

While the photoconductivity of the films could be improved in pure phases, the corresponding photoconductivity and long-lived component for n = 2 and n = 3 compositions are quite remarkable under these conditions, in line with their promising photovoltaic performance. These performances presently remain inferior to the 3D and 2D/3D perovskite solar cells, which can be ascribed to the challenges associated with the phase purity as well as the lower conductivity of the spacer layer that is particularly detrimental in the parallel orientation of the perovskite phases. Therefore, further control of the corresponding perovskite phase formation and orientation, along with optimizing the device architectures, could lead to improved photovoltaic performances of perovskite solar cells incorporating DJ phases in the future.

3. Conclusion

We investigated layered hybrid perovskites based on (PDMA)FA$_{n-1}$Pb$_n$I$_{3n+1}$ (n = 1–3) compositions to unravel the underlying structural and photophysical properties of these unique Dion-Jacobson phases that determine their photovoltaic performances. X-ray scattering measurements confirm presence of a layered structure for n = 1 and n = 2 nominal compositions, whereas mixtures of phases are apparent for n = 3 composition without evidencing the formation of higher n > 2 representatives.
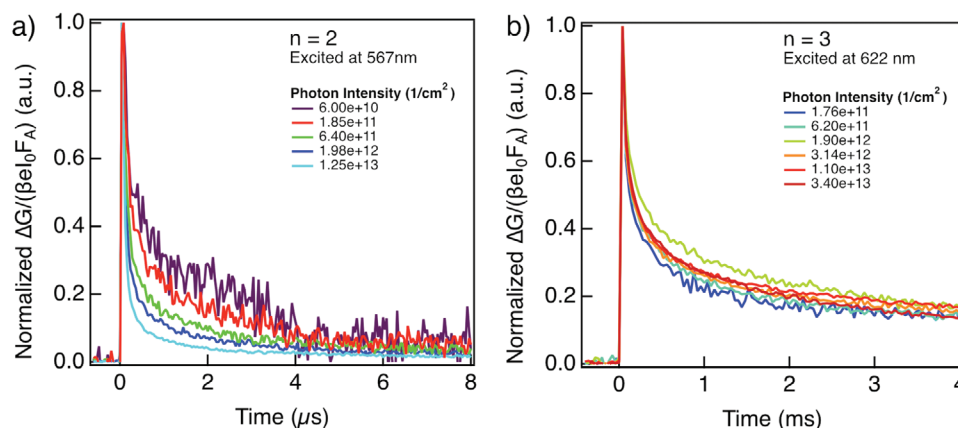
Figure 6. Charge carrier dynamics. Normalized photoconductivity as a function of photon intensity of $(PDMA)FA_{n-1}Pb_nI_{3n+1}$ thin films on quartz substrates based on a) $n = 2$ and b) $n = 3$ nominal compositions highlighting long lived-component in the order of µs–ms.

Molecular dynamics simulations and density functional theory calculations of Dion-Jacobson structures complement the experimental findings by elucidating intermolecular interactions and revealing less favorable formation enthalpies with increasing number of inorganic layers (n). Moreover, the subtle interaction between the organic moieties and hybrid perovskite layers were found to result in smaller interlayer distances and better alignment as compared to the Ruddlesden-Popper phases, resulting in lower effective masses for charge carriers. Consequently, despite the challenges in obtaining pure phases of $n > 1$ compositions, time-resolved microwave conductivity measurements reveal high photoconductivities and long charge carrier lifetimes in the order of hundreds of microseconds for $n \geq 2$ compositions that can account for the promising photovoltaic performances of these materials. This study thereby provides important new insights for the design of hybrid low-dimensional perovskite materials for optoelectronic applications.

4. Experimental Section

Synthesis and characterization of materials, as well as the corresponding methods are provided in the Supporting Information.

Supporting Information

Supporting Information is available from the Wiley Online Library or from the authors.

Conflict of Interest

The authors declare no conflict of interest.

Author Contributions

M.C.G.-R., P.A., and L.M. contributed equally to this work. The manuscript was written by J.V.M., L.M., F.J., P.A., M.M., and M.G-R. with the support of all authors. The project was conceptualized by J.V.M., who coordinated the investigation. M.C.G.-R. and F.C.G. performed the photoconductivity measurements and analysis of charge carrier dynamics with the support of W.T. while P.A., M.M., F.J., and U.R. performed, analyzed, and interpreted the molecular dynamics simulations and DFT calculations. L.M. and A.H. performed the X-ray scattering measurements and the analysis with the support of M.I.D. and F.S. while Y.L. and A.D. prepared the samples. A.D. analyzed substrate-dependent XRD patterns. A.U. conducted the XRD and PL spectroscopy. B.C., A.H., and S.M.Z. were involved in the discussion and provided support in project coordination, while M.G. directed the project.

[1] A. K. Jena, A. Kulkarni, T. Miyasaka, *Chem. Rev.* **2019**, *119*, 3036.
[2] M. Grätzel, *Acc. Chem. Res.* **2017**, *50*, 487.
[3] S. Kazim, M. K. Nazeeruddin, M. Grätzel, S. Ahmad, *Angew. Chem., Int. Ed.* **2014**, *53*, 2812.
[4] R. Wang, M. Mujahid, Y. Duan, Z.-K. Wang, J. Xue, Y. Yang, *Adv. Funct. Mater.* **2019**, *29*, 1808843.

[5] Y. Rong, Y. Hu, A. Mei, H. Tan, M. I. Saidaminov, S. I. Seok, M. D. McGehee, E. H. Sargent, H. Han, *Science* **2018**, *361*, eaat8235.

[6] J. V. Milić, D. J. Kubicki, L. Emsley, M. Grätzel, *Chim. Int. J. Chem.* **2019**, *73*, 317.

[7] B. Saparov, D. B. Mitzi, *Chem. Rev.* **2016**, *116*, 4558.

[8] L. Mao, C. C. Stoumpos, M. G. Kanatzidis, *J. Am. Chem. Soc.* **2019**, *141*, 1171.

[9] G. Grancini, M. K. Nazeeruddin, *Nat. Rev. Mater.* **2019**, *4*, 4.

[10] N. Mercier, *Angew. Chem., Int. Ed.* **2019**, *58*, 17912.

[11] a) G. Liu, H. Zheng, H. Xu, L. Zhang, X. Xu, S. Xu, X. Pan, *Nano Energy* **2020**, *73*, 104753; b) H. Zheng, W. Wu, H. Xu, F. Zheng, G. Liu, X. Pan, Q. Chen, *Adv. Funct. Mater.* **2020**, *30*, 2000034.

[12] C. C. Stoumpos, D. H. Cao, D. J. Clark, J. Young, J. M. Rondinelli, J. I. Jang, J. T. Hupp, M. G. Kanatzidis, *Chem. Mater.* **2016**, *28*, 2852.

[13] Y. Chen, Y. Sun, J. Peng, J. Tang, K. Zheng, Z. Liang, *Adv. Mater.* **2017**, *131*, 1703487.

[14] N. Wang, L. Cheng, R. Ge, S. Zhang, Y. Miao, W. Zou, C. Yi, Y. Sun, Y. Cao, R. Yang, Y. Wei, Q. Guo, Y. Ke, M. Yu, Y. Jin, Y. Liu, Q. Ding, D. Di, Le Yang, G. X , H. Tian, C. Jin, F. Gao, R. H. Friend, J. Wang, W. Huang, *Nat. Photonics* **2016**, *10*, 699.

[15] L. Mao, W. Ke, L. Pedesseau, Y. Wu, C. Katan, J. Even, M. R. Wasielewski, C. C. Stoumpos, M. G. Kanatzidis, *J. Am. Chem. Soc.* **2018**, *140*, 3775.

[16] Y. Li, J. V. Milić, A. Ummadisingu, J.-Y. Seo, J.-H. Im, H.-S. Kim, Y. Liu, M. I. Dar, S. M. Zakeeruddin, P. Wang, A. Hagfeldt, M. Grätzel, *Nano Lett.* **2019**, *19*, 150.

[17] B.-E. Cohen, Y. Li, Q. Meng, L. Etgar, *Nano Lett.* **2019**, *19*, 2588.

[18] X. Li, W. Ke, B. Traore, P. Guo, I. Hadar, M. Kepenekian, J. Even, C. Katan, C. C. Stoumpos, R. D. Schaller, M. G. Kanatzidis, *J. Am. Chem. Soc.* **2019**, *141*, 12880.

[19] Z. Xu, M. Chen, S. F. Liu, *J. Phys. Chem. Lett.* **2019**, *10*, 3670.

[20] Y. Zheng, T. Niu, J. Qiu, L. Chao, B. Li, Y. Yang, Q. Li, C. Lin, X. Gao, C. Zhang, Y. Xia, Y. Chen, W. Huang, *Sol. RRL* **2019**, *3*, 201900090.

[21] G. Li, T. Zhang, N. Guo, F. Xu, X. Qian, Y. Zhao, *Angew. Chem., Int. Ed.* **2016**, *55*, 13460; *Angew. Chem.* **2016**, *128*, 13658.

[22] J. Yan, W. Fu, X. Zhang, J. Chen, W. Yang, W. Qiu, G. Wu, F. Liu, P. Heremans, H. Chen, *Mater. Chem. Front.* **2017**, *2*, 121.

[23] H. Zheng, G. Liu, L. Zhu, J. Ye, X. Zhang, A. Alsaedi, T. Hayat, X. Pan, S. Dai, *Adv. Energy Mater.* **2018**, *8*, 1800051.

[24] J. V. Milić, J.-H. Im, D. J. Kubicki, A. Ummadisingu, J.-Y. Seo, Y. Li, M. A. Ruiz Preciado, M. I. Dar, S. M. Zakeeruddin, L. Emsley, M. Grätzel, *Adv. Energy Mater.* **2019**, *9*, 1900284.

[25] A. Q. Alanazi, D. J. Kubicki, D. Prochowicz, E. A. Alharbi, M. E. F. Bouduban, F. Jahanbakhshi, M. Mladenović, J. V. Milić, F. Giordano, D. Ren, A. Y. Alyamani, H. Albrithen, A. Albadri, M. H. Alotaibi, J.-E. Moser, S. M. Zakeeruddin, U. Rothlisberger, L. Emsley, M. Grätzel, *J. Am. Chem. Soc.* **2019**, *141*, 17659.

[26] D. H. Cao, C. C. Stoumpos, O. K. Farha, J. T. Hupp, M. G. Kanatzidis, *J. Am. Chem. Soc.* **2015**, *137*, 7843.

[27] L. N. Quan, M. Yuan, R. Comin, O. Voznyy, E. M. Beauregard, S. Hoogland, A. Buin, A. R. Kirmani, K. Zhao, A. Amassian, D. H. Kim, E. H. Sargent, *J. Am. Chem. Soc.* **2016**, *138*, 2649.

[28] J. Liu, J. Leng, K. Wu, J. Zhang, S. Jin, *J. Am. Chem. Soc.* **2017**, *139*, 1432.

[29] A. H. Proppe, R. Quintero-Bermudez, H. Tan, O. Voznyy, S. O. Kelley, E. H. Sargent, *J. Am. Chem. Soc.* **2018**, *140*, 2890.

[30] M. C. Gélvez-Rueda, E. M. Hutter, D. H. Cao, N. Renaud, C. C. Stoumpos, J. T. Hupp, T. J. Savenije, M. G. Kanatzidis, F. C. Grozema, *J. Phys. Chem. C* **2017**, *121*, 26566.

[31] R. Herckens, W. T. M. Van Gompel, W. Song, M. C. Gélvez-Rueda, A. Maufort, B. Ruttens, J. D'Haen, F. C. Grozema, T. Aernouts, L. Lutsen, D. Vanderzande, *J. Mater. Chem. A* **2018**, *6*, 22899.

[32] D. B. Mitzi, *J. Chem. Soc., Dalton Trans.* **2001**, *1*, https://doi.org/10.1039/b007070j.

[33] S. Ahmad, P. Fu, S. Yu, Q. Yang, X. Liu, X. Wang, X. Wang, X. Guo, C. Li, *Joule* **2019**, *3*, 794.

[34] N. Ashari-Astani, F. Jahabakhshi, M. Mladenović, A. Q. M. Alanazi, I. Ahmadabadi, M. R. Ejtehadi, M. I. Dar, M. Grätzel, U. Rothlisberger, *J. Phys. Chem. Lett.* **2019**, *10*, 3543.

[35] a) C. Yi, J. Luo, S. Meloni, A. Boziki, N. Ashari-Astani, C. Grätzel, S. M. Zakeeruddin, U. Rothlisberger, M. Grätzel, *Energy Environ. Sci.* **2016**, *9*, 656; b) Z. Wang, Q. Lin, F. P. Chmiel, N. Sakai, L. M. Herz, H. J. Snaith, *Nat. Energy* **2017**, *2*, 17135.

[36] H. Tsai, W. Nie, J.-C. Blancon, C. C. Stoumpos, R. Asadpour, B. Harutyunyan, A. J. Neukirch, R. Verduzco, J. J. Crochet, S. Tretiak, L. Pedesseau, J. Even, M. A. Alam, G. Gupta, J. Lou, P. M. Ajayan, M. J. Bedzyk, M. G. Kanatzidis, A. D. Mohite, *Nature* **2016**, *536*, 312.

[37] L. Gan, J. Li, Z. Fang, H. He, Z. Ye, *J. Phys. Chem. Lett.* **2017**, *8*, 5177.

[38] J. C. Blancon, H. Tsai, W. Nie, C. C. Stoumpos, L. Pedesseau, C. Katan, M. Kepenekian, C. M. M. Soe, K. Appavoo, M. Y. Sfeir, S. Tretiak, P. M. Ajayan, M. G. Kanatzidis, J. Even, J. J. Crochet, A. D. Mohite, *Science* **2017**, *355*, 1288.